Benchtop Models of LISA Interferometry at the University of Florida

James I. Thorpe, Rachel J. Cruz, Shawn Mitryk, G.T.S. Reddy, and Guido Mueller
Department of Physics
University of Florida
PO Box 118440 Gainesville, FL 32611

***Abstract*—The Laser Interferometer Space Antenna (LISA) is a joint effort of NASA and the European Space Agency (ESA) to build and operate a space-based detector of gravitational waves. Along with ground-based observatories, LISA will launch the new field of gravitational wave astronomy, which promises to provide important insights in many areas of astronomy and cosmology. LISA will consist of a constellation of three satellites in a triangular configuration five million kilometers on a side. Laser interferometry will be used to monitor changes in the distance between the satellites at a level of $10\,\mathrm{pm}/\sqrt{\mathrm{Hz}}$ in an effort to detect small fluctuations induced by gravitational waves. Achieving such precise distance measurements over large distances requires a number of novel measurement techniques and technologies. Our group at the University of Florida is developing UFLIS (the University of Florida LISA Interferometry Simulator), a laboratory model which faithfully reproduces most aspects of the LISA interferometer. UFLIS is being used to study various aspects of LISA interferometry ranging from general measurement techniques to specific hardware implementations. In this paper we describe UFLIS in general with an emphasis on the technology we have developed. This work is supported by NASA/OSS grant BEFS04-0019-0019.**

I. Gravitational Waves and Their Detection

Nearly a century ago, Einstein recognized a wave solution to his equations of General Relativity in vacuum. Over the intervening decades, much theoretical work has deepened our understanding of these solutions, known as gravitational waves (GWs). The gravitational analog to electromagnetic radiation, GWs are disturbances in space-time which propagate through the universe at the speed of light. They are generated in some of the most violent and interesting events in our universe: colliding black holes and neutron stars, supernovae, and the Big Bang. For many astrophysical systems, GWs play a role that is at least as important as electromagnetic radiation. The observation of GWs will likely provide new insights in many fields of astronomy and astrophysics [1].

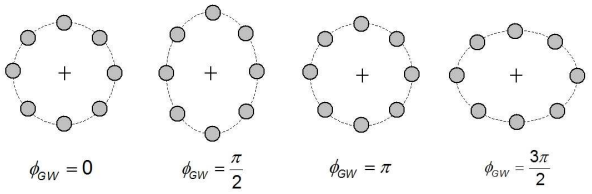

Figure 1. Tidal distortions cased by a "+ polarized" GW propagating normal to the figure plane

GWs may be observed by detecting the minute tidal distortions they cause in our local spacetime. Figure 1 shows the effect of a GW passing through an initially-circular ring of freely-falling test particles. The GW is propagating normal to the plane of the figure and ϕ_{GW} refers to the GW phase. The amplitude of a GW is characterized by its *strain*, a dimensionless number describing the change in displacement between two test-particles over their initial displacement. For typical astrophysical sources of GWs, the strains at Earth are expected to be on the order of 10^{-21}.

Generally speaking, there are two primary challenges in direct GW detection. The first is build test masses that are sufficiently isolated from their environment so that the disturbances caused by GWs are not overwhelmed by non-inertial forces. The second is to measure the distance between these masses with enough precision to resolve the small distortions caused by the GWs.

II. LISA

Like electromagnetic waves, expected GW sources span a large spectrum of frequencies. Accessing all of the interesting frequency bands will require the construction of a number of different types of GW detectors. Current and future ground-based detectors [2] will be limited to high frequency GWs ($f_{GW} \gtrsim 10\,\mathrm{Hz}$) due to the interference caused by Earth's fluctuating gravitational field. Observing the many interesting low-frequency sources will require a space-based gravitational wave detector.

The Laser Interferometer Space Antenna (LISA), is a joint NASA/ESA mission with the goal of studying GWs in the $10^{-4}\,\mathrm{Hz} \leq f_{GW} \leq 10^{-1}\,\mathrm{Hz}$ frequency band [3]. Target sources include colliding super-massive black holes in distant galaxies, binary compact objects in our own galaxy, and the capture of small compact objects by super-massive black holes. The LISA mission concept calls for placing three separate spacecraft (SC) in a set of heliocentric orbits such that they form a giant triangular constellation approximately $5 \times 10^9\,\mathrm{m}$ on a side, as depicted in Figure 2. Each SC will carry a pair of freely-floating *proof masses* surrounded by electrostatic sensors. These sensors will provide an input to a control system that fires miniature thrusters on the spacecraft to ensure that the SC remains centered around the proof masses [4]. Roughly speaking, the SC provides a shield from outside

disturbances so that the proof masses closely approximate the inertial test particles in Figure 1.

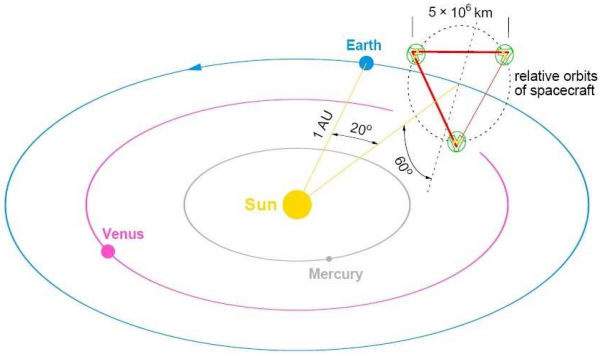

Figure 2. The LISA orbital configuration. (Courtesy NASA)

In order to detect GWs, changes in the distance between the proof masses must be measured at a level of roughly $10\,\mathrm{pm}/\sqrt{\mathrm{Hz}}$ ($5 \cdot 10^9\,\mathrm{m} \times 10^{-21} \approx 10\,\mathrm{pm}$).

Laser interferometry is a measurement technique which is ideal for measuring such small distances. In traditional interferometers, a single light source is split into two nearly equal paths and then recombined on a single detector. In this arrangement, the phase noise of the laser light source is common to both arms and is not measured at the detector. The LISA interferometer differs from a traditional interferometer in that it uses six separate light sources and eighteen independent measurement points. The signals from these measurement points are then combined electronically to produce measurement channels that have the noise-suppression properties of a traditional interferometer.

Figure 3 shows a diagram of the LISA interferometer. The three SC are labeled SC_i and lie on the vertices of an approximately-equilateral triangle. Each SC contains two optical benches (OBs) consisting of a proof mass, laser, and photoreceiver. In Figure 3, OB_{ij} refers to the OB on SC_i oriented towards SC_j. The distances between the SC are denoted by τ_{ij} , the time for a photon to travel from SC_i to SC_j. In addition to the free-space links between the SC, the two OBs on each SC are connected via an optical fiber.

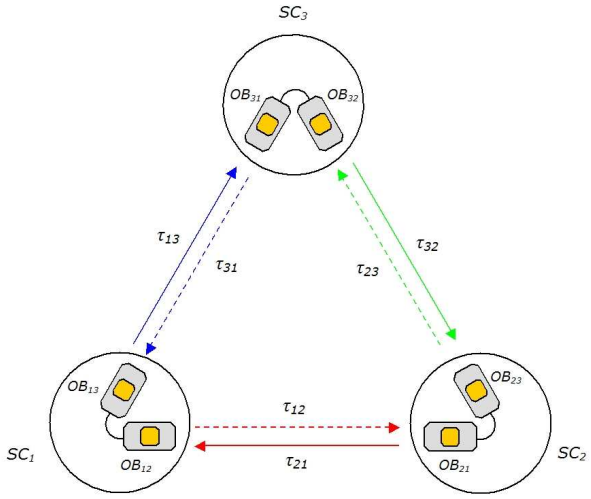

Figure 3. Schematic diagram of the LISA interferometer. (SC = spacecraft, OB = optical bench, τ_{ij} = light travel time between SC_i and SC_j)

One possible layout of the the optical bench is depicted in Figure 4. At each of the three photodiodes (PDs), a pair of laser beams is interfered, producing a signal of the form

$$P(t) \propto \sin[2\pi\Delta\nu t + \Delta\phi(t)], \tag{1}$$

where $P(t)$ is the power on the photodiode, $\Delta\nu$ is the frequency difference between the two laser beams, and $\Delta\phi(t)$ is the phase difference between the two laser beams. The photodiode signal is connected to a device known as a *phasemeter* which extracts $\Delta\phi(t)$ from the signal[1].

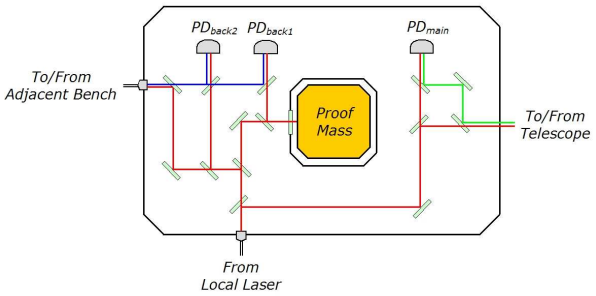

Figure 4. Diagram of a LISA optical bench. Light from the local laser (red) enters from the fiber coupler on the bottom, light from the adjacent optical bench (blue) enters from the left, and light from the far spacecraft (green) enters from the right.

A pair of local interferometers are used to measure the relative motion between the proof mass and the OB. PD_{back2} measures the phase difference between the local laser and the laser from the adjacent OB. PD_{back1} makes the same measurement, with the slight difference that the local beam is

[1]Note that there is an equivalency between phase and frequency which allows for all time-variation in the signal to be placed in $\Delta\phi(t)$ while allowing $\Delta\nu$ to be chosen as an arbitrary constant.

reflected off of the proof mass. By differencing the phasemeter signals from PD_{back1} and PD_{back2}, the relative motion between the proof mass and OB can be measured. Key to the success of this measurement is a phasemeter with sufficient dynamic range to capture the laser phase noise on the individual PDs while still providing enough resolution to resolve length changes of $10\,\mathrm{pm}/\sqrt{\mathrm{Hz}}$.

A. Time-Delay Interferometry

Relative motion between the OBs on separate SC is measured using PD_{main}, which compares the local laser beam with an incoming beam from the far SC. The phasemeter output from PD_{main} on OB_{ij} is

$$S_{ij}(t) = \phi_{ij}(t) - \phi_{ji}(t - \tau_{ji}) + h_{ji}(t), \tag{2}$$

where $\phi_{ij}(t)$ is the phase noise of the laser on OB_{ij} and $h_{ij}(t)$ is the accumulated phase due to GWs for a beam traveling from SC_i to SC_j. Since the two laser phase noise terms are uncorrelated, they will not cancel and hence will dominate the phasemeter output, obscuring the GW signal. However, it is possible to form combinations of $S_{ij}(t)$ from different optical benches with appropriate time delays that do cancel the laser phase noise and reveal the GW signals. This technique is known as time-delay interferometry (TDI) [5].

As an example of TDI, consider the simplified case where the signals $S_{j1}(t)$ are used as error signals in a phase-lock loop that adjusts the phase $\phi_{j1}(t)$. For high gains, $S_{j1}(t) \approx 0$ and consequently

$$\phi_{ji}(t) \approx \phi_{1j}(t - \tau_{1j}) + h_{j1}(t). \tag{3}$$

In other words, SC_2 and SC_3 act as transponders: repeating the phase of the incoming signal from SC_1. The phasemeter signals at SC_1 are then

$$S_{1j}(t) = \phi_{1j}(t) - \phi_{1j}(t - \tau_{1j} - \tau_{j1}) + h(t - \tau_{j1}) + h_{j1}(t). \tag{4}$$

An additional simplification can be made by phase-locking the two lasers on SC_1 using the two PD_{back2} signals. The phasemeter output from PD_{back2} on each bench will contian the difference in laser phases, $\Delta\phi_1(t) \equiv \phi_{12}(t) - \phi_{13}(t)$, plus a phase noise, $\eta(t)$, added by the optical fiber link. $\Delta\phi_1(t)$ will appear with opposite signs on the two optical benches while $\eta(t)$ will have the same sign. Differencing the two phasemeter signals will result in a signal proportional to $\Delta\phi_1(t)$ with no contribution from $\eta(t)$. This signal can be used as an error signal in a phase-lock loop which adjusts the phase of $\phi_{13}(t)$. Under the assumption of high gain, this implies

$$\phi_{13}(t) \approx \phi_{12}(t) \equiv \phi(t). \tag{5}$$

This is analogous to a beamsplitter producing two coherent beams for each optical bench. The signals $S_{1j}(t)$ can then be combined to form the 'Michelson X' TDI combination,

$$X(t) \equiv S_{12}(t) - S_{13}(t) - S_{12}(t - \tau_{13} - \tau_{31}) + S_{13}(t - \tau_{12} - \tau_{21}). \tag{6}$$

Substituting (4) into (6) gives

$$\begin{aligned} X(t) \;=\; & h_{21}(t) - h_{31}(t) + h_{12}(t - \tau_{21}) - h_{13}(t - \tau_{31}) \\ & - h_{21}(t - \tau_{13} - \tau_{31}) + h_{31}(t - \tau_{12} - \tau_{21}) \\ & - h_{12}(t - \tau_{21} - \tau_{13} - \tau_{31}) + h_{31}(t - \tau_{12} - \tau_{31}). \end{aligned} \tag{7}$$

There are no contributions from laser phase noise in $X(t)$. Physically, this is equivalent to the situation in an equal-arm Michelson interferometer. It should be noted that the phase lock loops implied in equations (3) and (5) are not critical to the success of TDI. It is possible to form a more-general expression for $X(t)$ using the $S_{ji}(t)$ signals and the PD_{back1} signals that does not require any PLLs.

B. Pre-Stabilization and Arm-Locking

In principle, the cancellation of laser phase noise in (7) is perfect, placing no constraints on the performance of the lasers. In practice, the cancellation is only approximate due to such effects as length changes in the arms due to orbital motion, errors in determining the arm-length, and errors in generating time-delayed copies of the phasemeter signals. These effects allow some laser phase noise to enter the TDI channels. With unstabilized lasers, the post-TDI residuals are too large to permit detection of GWs, therefore it is necessary to actively stabilize the phase (or frequency) of the lasers prior to forming the TDI combinations.

LISA will stabilize its lasers in two stages. The first stage, called pre-stabilization, utilizes a high-finesse optical cavity as a frequency reference. Standard locking techniques, such as the RF demodulation technique known as Pound-Drever-Hall locking [6], can be used to transfer the length stability of the cavity spacer to frequency stability of the laser. The performance of the pre-stabilization system is ultimately limited by the length stability of the cavity spacer. Using ultra-stable materials in a thermally-stabilized environment, it is expected that the pre-stabilization will provide a frequency stability of roughly $10\,\mathrm{Hz}/\sqrt{\mathrm{Hz}}$ in the LISA measurement band [7].

Improvement upon the pre-stabiliztion requires a length or frequency reference with better stability than the optical cavity spacer. The arms of the LISA constellation fit this description in the frequency band of interest ($\gtrsim 10^{-4}\,\mathrm{Hz}$). Arm-locking [8] is a techniuqe where by the laser is stabilized to one or more of the LISA arms.

In its simplest incarnation, single-arm arm-locking, one laser is stabilized to a single arm. As an example, consider the laser on OB_{12} and let the phase-lock condition in (3) be applied on OB_{21}. The phasemeter signal at PD_{main} on OB_{12} is given by (4), which we can re-write as

$$S(t) = \phi(t) - \phi(t - \tau_{RT}), \tag{8}$$

where $\tau_{RT} \equiv \tau_{12} + \tau_{21}$ is the round-trip light travel time between SC_1 and SC_2, the small GW contributions have been dropped, and the ij indices have been dropped for clarity. The sensitivity of $S(t)$ to variations in laser phase will depend on the frequency of the variation. A sinusoidal variation in phase with a frequency of $n/\tau_{RT},\ n \in 1, 2, 3\ldots$ will not produce a change in $S(t)$. Similarly, a sinusoidal phase variation with a frequency of $(n + \frac{1}{2})/\tau_{RT},\ n \in 1, 2, 3\ldots$ will produce a signal in $S(t)$ with an amplitude twice that of the original variation. This is more easily seen by expressing (8) in the Fourier domain,

$$\tilde{S}(f) = \tilde{\phi}(f) \cdot [1 + \exp(-2\pi i f \tau)], \tag{9}$$

where $\tilde{S}(f)$ and $\tilde{\phi}(f)$ are the Fourier transforms of $S(t)$ and $\phi(t)$, and f is the Fourier frequency. A Bode plot of $\tilde{S}(f)/\tilde{\phi}(f)$, the "error signal transfer function", is shown in Figure 5. The error signal goes to zero at Fourier frequencies $f_n \equiv n/\tau_{RT}$. As it approaches these same frequencies, the phase of the error signal transfer function approaches $-90°$. When coupled with the $-90°$ phase response of the laser phase actuator, these points amount to sign changes in the error signal. In the language of control theory, they are marginally-stable points and in practice will cause a control system utilizing this error signal to be unstable.

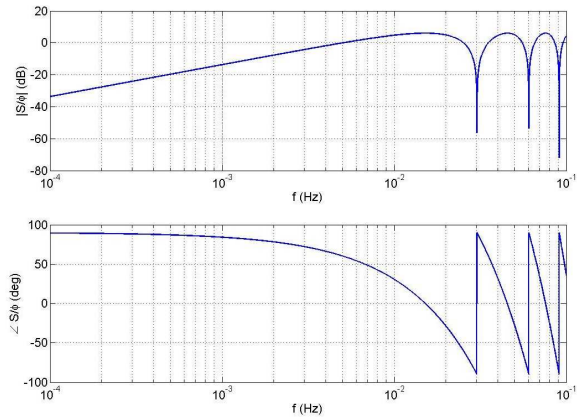

Figure 5. Bode plot of single-arm arm-locking error signal transfer function

The standard practice for dealing with such instabilities is to ensure that the control system has no gain at these frequencies. Unfortunately for arm-locking, the instabilities lie in the LISA band, precisely where gain is needed. The resolution to this problem comes in utilizing a controller[2] that has a frequency response of the form

$$G(f) = G_0(2\pi i f)^p, \tag{10}$$

where G_0 is an overall gain factor and p is a coefficient in the range $0.2 \lesssim p \lesssim 0.8$, in the vicinity of the instability points. This controller will provide a "phase advance" at $f = f_n$, allowing the system to remain stable. At other frequencies, notably for $f < f_1$, the coefficient p can become negative, providing improved noise suppression. The closed-loop noise suppression for an arm-locking system is shown schematically in Figure 6. For frequencies below f_1, there is large noise suppression. As f approaches f_1, the noise increases and actually exceeds the input noise (a condition known as noise enhancement) for a brief period before entering a second noise suppression region. This pattern repeats at each f_n until the unity-gain frequency, the maximum frequency at which the control loop is active, is reached.

It should be noted that the curve shown in Figure 6 is only qualitative, for realistic arm-locking systems, the noise enhancement spikes will be narrower, the noise suppression regions deeper, and the unity-gain frequency higher. While arm-locking does not suppress noise at all-frequencies, it greatly improves the frequency stability in large frequency bands. In actual practice, LISA will probably utilize more complex arm-locking schemes involving multiple arms. These schemes will allow the noise spikes to be moved to higher frequencies, providing consistent stability in the LISA measurement band.

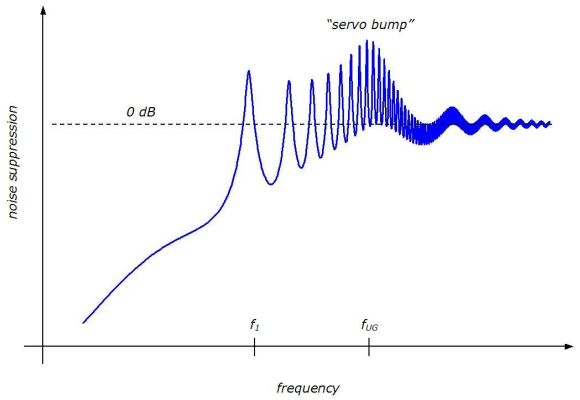

Figure 6. Qualitative depiction of closed-loop noise suppression for an arm-locking system. $f_1 = f/\tau_{RT}$, f_{UG}= unity gain frequency.

III. UFLIS

The "one-shot" nature of space-based instruments makes the pre-flight validation of measurement techniques and technologies an extremely important aspect of the mission. Such pre-flight testing is especially challenging for LISA due to the fact that the large size of the constellation is an essential feature of the mission. While most of the individual components can be verified in compartmentalized tests, system-level technologies such as TDI and arm-locking need to be verified on a model of the complete interferometer. At the University of Florida, a group of researchers are developing a hardware-based model know as the University of Florida LISA Interferometry Simulator (UFLIS). The goal of UFLIS is to create a system with signals that have transfer functions and noise characteristics that are similar to those found in LISA [9], [10], [11].

For the most part, UFLIS replicates the LISA interferometer using a one-to-one correspondence between parts. The lasers, phasemeters, and control systems are similar to those that will be used in LISA. The large inter-SC distance is modeled using a technique called Electronic Phase Delay (EPD), which uses a digital delay line to delay a signal containing LISA-like noise [12]. An example of the EPD technique applied to a single LISA arm is shown in Figure 7.

Figure 7(a) shows a model of a LISA arm. Laser L_1, onboard SC_1, produces a light field with frequency ν_1 and phase $\phi_1(t)$ which propagates to SC_2 and experiences a delay

[2]In some of the literature, the laser actuator, which has an integrator response of the form $(2\pi i f)^{-1}$, is absorbed into the controller response. Here we treat the controller and actuators as separate components.

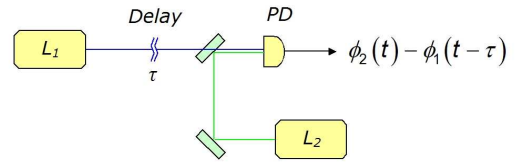

(a) LISA

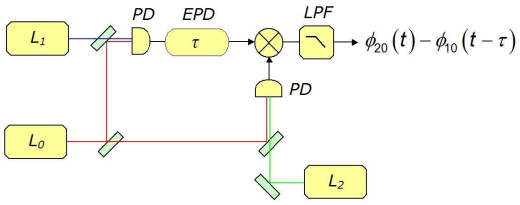

(b) EPD Model

Figure 7. The EPD technique applied to a single LISA arm

τ. Upon arrival on SC_2, it is interfered with the local laser on the optical bench, L_2, producing a signal with a frequency

$$\nu_{LISA} = \nu_2 - \nu_1 - \nu_{Doppler}, \tag{11}$$

where $\nu_{Doppler}$ is the Doppler shift. The phase of the signal will be

$$\phi_{LISA}(t) = \phi_2(t) - \phi_1(t-\tau), \tag{12}$$

where the small phase shifts due to GWs have been ignored. The EPD model of Figure 7(a) is shown in Figure 7(b). Two identical, uncorrelated lasers, L_1 and L_0, are interfered at a photodiode, producing a beat signal with a frequency $\nu_{10} = \nu_1 - \nu_0$ and a phase $\phi_{10}(t) = \phi_1(t) - \phi_0(t)$. If the noise spectra of L_1 and L_0 are identical and uncorrelated, the phase noise of the beat note will approximately equal that of L_1,

$$\tilde{\phi}_{10}(f) = \sqrt{\tilde{\phi}_1^2(f) + \tilde{\phi}_0^2(f)} \approx \tilde{\phi}_1(f),\ \tilde{\phi}_0(f) \lesssim \tilde{\phi}_1(f). \tag{13}$$

In the EPD model, the $L_1 - L_0$ beat note represents L_1 in LISA. The noise spectra of the two signals are the same, the only difference being that the EPD signal is at a much lower frequency and can be easily converted to an electronic signal.

The next step in the EPD model is to measure the $L_1 - L_0$ beat note and store it in a delay buffer for a time τ to model the light propagation between the SC. Additionally, it is possible to add a frequency shift to the signal, mimicking the Doppler effect present in LISA. The output of the EPD unit is a signal with frequency $\nu_{10} + \nu_{Doppler}$ and phase $\phi_{10}(t-\tau)$. The next step is to model the local laser onboard SC_2. This is done by making a beat note between a third laser, L_2, and the reference laser, L_0. In principle the reference laser could be an entirely separate laser but for convenience, the same laser is used. This produces a beat signal with frequency ν_{20} and phase ϕ_{20}. This signal is then electronically mixed with the output of the EPD unit. After low-pass filtering to remove high-frequency terms, the output of the mixer is a signal with frequency

$$\nu_{EPD} = \nu_{20} - \nu_{10} - \nu_{Doppler} \tag{14}$$

and phase

$$\phi_{EPD}(t) = \phi_{20}(t) - \phi_{10}(t-\tau). \tag{15}$$

So long as the laser phase noise remains uncorrelated and $\tilde{\phi}_0(f)$ is sufficiently small, (14) and (15) have exactly the same characteristics as (11) and (12).

The EPD model of a single arm can easily be extended to model the entire LISA constellation. Figure 8 shows the current optical layout of UFLIS [10]. Two lasers, L_1 and L_0 are stabilized to ultra-stable optical cavities placed in a thermally-isolated vacuum chamber. The residual phase noise of these lasers meets the LISA pre-stabilization requirement. Two additional lasers, L_2 and L_3 allow the modeling of the LISA arms. Each laser is interferred with L_0, producing an electronic beat signal which can be used to model a LISA laser. This allows the study of arm-locking, various TDI combinations, and verification of components such as phasemeters.

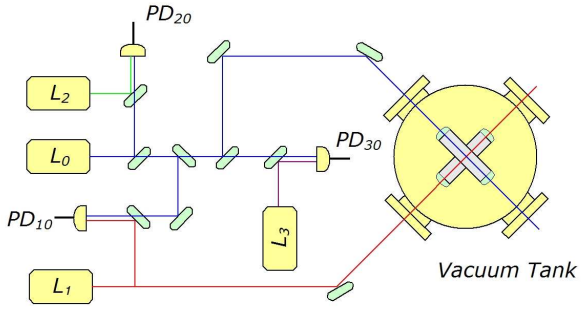

Figure 8. Optical layout of UFLIS, L_0 is the reference laser, L_1-L_3 represent the LISA lasers, and PD_ij are beat notes between L_i and L_j.

IV. UFLIS Technology

The development of UFLIS necessitated the development of a number of technologies, some of which are also common to LISA and others which are unique to the modeling technique.

A. Phasemeters

As described in section II, the phasemeter is a critical component in the LISA interferometric measurement system. In order to resolve the phase changes induced by GWs on the optical beat signals, it must be able to measure the phase of the beat signal with an accuracy of $\sim 10^{-6}$ cycles/$\sqrt{\text{Hz}}$. This accuracy must be achieved in the presence of laser phase noise with an RMS phase noise of greater than 10^6 cycles in the LISA band. In addition, the frequency of the beat signals will slowly vary by as much as 10 MHz due to the Doppler shifts induced by orbital motion.

The current design for both the LISA phasemeter [13] and the UFLIS phasemeter [11] is an in-phase/quadrature (I/Q) demodulation phasemeter with a tracking local oscillator (LO). A schematic of such a system is shown in Figure 9. The input signal, a sinusoid with amplitude $A_i(t)$, frequency ν_i,

and phase $\phi_i(t)$, enters from the top left and is multiplied by both quadratures of a local reference oscillator (LO), with unit amplitude, frequency ν_m, and phase $\phi_m(t)$. Without loss of generality, we can assume that $\nu_m = \nu_i$ and place all differences between the input signal and LO in the phase terms. The outputs of the two multipliers is low-pass filtered to remove harmonics at $2\nu_i$ and scaled by a factor of 2, resulting in the signals

$$I(t) = A_i(t)\cos\left[\phi_i(t) - \phi_m(t)\right] \tag{16}$$

and

$$Q(t) = A_i(t)\sin\left[\phi_i(t) - \phi_m(t)\right]. \tag{17}$$

These signals can be used to extract both the amplitude and the phase of the incoming signal,

$$A_i(t) = \sqrt{I(t)^2 + Q(t)^2} \tag{18}$$

and

$$\phi_i(t) = \arctan\left[Q(t)/I(t)\right]. \tag{19}$$

The last relationship will only unambiguously resolve the phase if it can be ensured that $|\phi_i(t) - \phi_m(t)| \leq \frac{1}{2}$ cycle. For the large phase noises present in the LISA beat signals, $\phi_i(t)$ will change by $\sim 10^6$ cycles, making it impossible to extract usin (19). The solution is to adjust the phase of the LO to ensure than the residual phase, $\phi_r(t) \equiv \phi_i(t) - \phi_m(t)$, remains within $\pm\frac{1}{2}$ cycle. This can be done by using ϕ_r as the error signal in a phase lock loop with a feedback gain $H(s)$ as shown in the Figure. For most LOs, the actuator is a frequency actuator rather than a phase actuator, hence an implicit integrator ($1/s$ in the Laplace domain) must be added to the control loop. The input phase of the original signal can be recovered by integrating the actuator signal to recover $\phi_m(t)$ and then adding the residual phase to recover the phase of the input signal. This process is known as phase reconstruction. In practice, an overall offset frequency, ν_{off}, is added to the LO outside the phase-lock loop. This is a reference frequency which the phasemeter will measure all phases with respect to. For example, if the reference frequency is 10 MHz and an input signal with a frequency of 11 MHz is applied to the input, the output of the phasemeter will be a continuous ramp with a slope of 10^6 cycles/s.

The UFLIS phasemeter is implemented in a digital signal-processing unit consisting of a FPGA which handles the I/Q demodulation and the phase-lock loop and a floating-point processor which handles scaling and phase reconstruction. Inputs are sampled at 100 MHz and multiplied with LO signals from a direct digital synthesizer (DDS). The outputs of the multipliers are digitally filtered and downsampled to approximately 800 kHz. Rather than implement (19) in the FPGA, the $Q(t)$ signal is used as the error signal in the phase-lock loop, which has a unity gain bandwidth of approximately 8 kHz. The $I(t)$, $Q(t)$, and $\nu_{corr}(t)$ signals are further downsampled to approximately 100 kHz and transferred to the floating point processor. The floating point processor reconstructs the phase and amplitude of the signal, filters and downsamples them further, and transfers the data to a host PC.

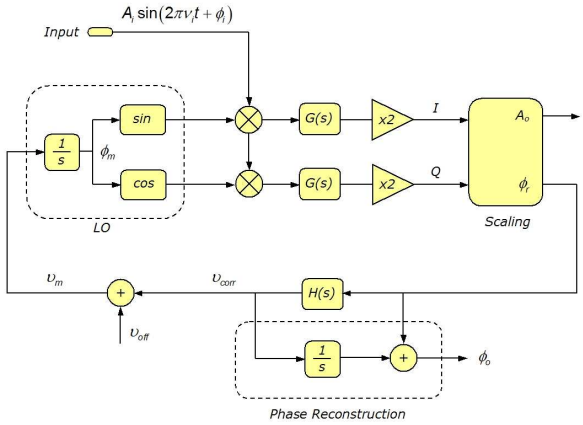

Figure 9. Schematic of an I/Q phasemeter with a tracking LO

The performance of the UFLIS phasemeter was evaluated using an "entangled-phase" test, designed to mimic the requirements of TDI. Three independent electrical oscillators with phases $\phi_i(t)$ $i = 1, 2, 3$ were mixed pair wise, creating three electronic beat signals with phases $\phi_{ij}(t) \equiv \phi_i(t) - \phi_j(t)$, $i < j$. These phases of the three beat signals were measured using three independent phasemeter channels. The measured signals were then combined in a phase-noise canceling linear combination,

$$\phi_{123}(t) \equiv \phi_{12}(t) + \phi_{13}(t) - \phi_{23}(t) = 0. \tag{20}$$

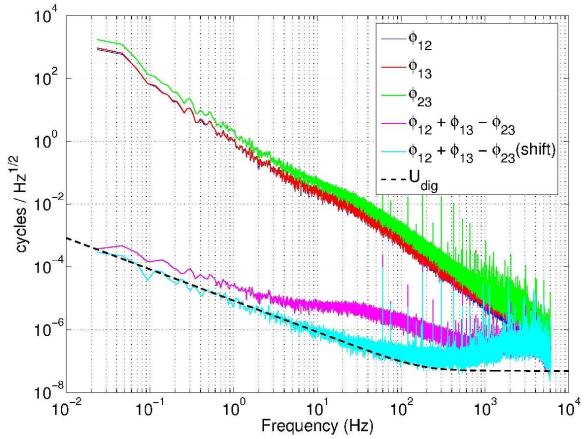

Figure 10. Performance of the UFLIS phasemeter in an entangled-phase measurement

Figure 10 shows the results of the measurement. The three individual beat note signals have the noise spectra in the upper curves. The magenta curve shows $\tilde{\phi}_{123}(f)$ obtained using the raw phasemeter outputs. The cyan curve shows $\tilde{\phi}_{123}(f)$ after correcting for a fixed time-delay between the three phasemeter channels using a fractional-delay interpolation filter [14]. The corrected result follows the theoretical prediction of the noise added by finite representation of the DDS frequency, indicating that the UFLIS phasemeter is currently limited by digitization

noise. This can be corrected by increasing the number of bits in the DDS, a process which is currently ongoing.

B. EPD Units

One piece of technology which is necessary for UFLIS but not for LISA is the EPD unit. The EPD units were developed in three generations [11]. The initial iteration of the EPD unit was a simple digital delay line consisting of an analog/digital converter (ADC), a first-in first-out (FIFO) memory buffer, and a digital/analog converter (DAC) all driven by a single sampling clock. The maximum sampling frequency was 200 kHz, too slow for LISA beat notes but acceptable for proof-of-concept. A total of 64 MB of RAM was capable of storing each of the two independent channels for up to 80 s.

The second-generation utilized the same general architecture but was transferred to hardware capable of digitizing four channels at up to 25 MHz. The increase in sampling frequency also increased the memory requirements, resulting in a maximum delay of $\sim$ 3 s for each channels with the 1 GBmemory capacity.

A change in architecture was made for the third-generation EPD unit. Rather than digitize and store the entire time-series of the beat note, a phasemeter is used to measure $I(t)$,$Q(t)$, and $\nu_{corr}(t)$ of the beat note. These signals are then downsampled to $\sim$ 100 kHz and stored in a FIFO buffer. The output of the buffer is connected to a second DDS, which produces a copy of the delayed signal that is fed to a DAC. This arrangement greatly reduces the data storage requirements of the EPD unit. It also allows for a frequency shift to be induced between the two signals by using a different offset frequency in the phasemeter and the output DDS. The trade-off is that phase or amplitude information at frequencies above $\sim$ 50 kHz is filtered out by the EPD unit. This is not an issue for the LISA science signals, which are in the mHz band, or arm-locking loops, which typically have unity gain bandwidths of $\leq$ 10 kHz.

V. Preliminary Results with UFLIS

A. TDI

The initial test of TDI-principles with UFLIS was a "single-arm TDI" experiment performed with the second-generation EPD unit and an earlier version of the UFLIS phasemeter that operated on signals in the 10 kHz range [15]. A diagram of the experiment is shown in Figure 11. Two pre-stabilized lasers are interfered at a PD, producing a beat note with a frequency of $\sim$ 10 MHz. To bring the frequency into the range of the second-generation EPD unit, the beat note is demodulated using LO_1, a mixer, and a low-pass filter. The result is a signal with a frequency of $\sim$ 1 MHz and phase noise of a pre-stabilized laser. This signal is electronically split into two portions, one of which is delayed by $\tau \approx 2$ s in the EPD unit. Both the output of the EPD unit and the un-delayed signal are again demodulated using LO_2, producing two signals at $\sim$ 10 kHz. The phase of these signals is recorded using the phasemeters.

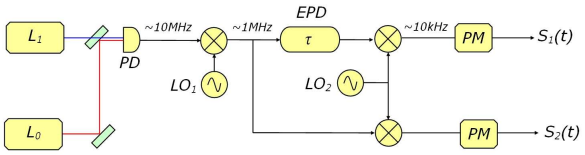

Figure 11. "Single-arm TDI" experiment using UFLIS

Figure 12 shows the results of the measurement. The curves labeled "prompt" and "delayed" show the noise spectra of the individual signals $S_1(t)$ and $S_2(t)$. The curve labeled "time-delayed combination" is the noise spectrum of the signal $S_1(t) - S_2(t - \tau\prime)$, where $\tau\prime$ is a time-delay chosen to match the EPD time delay, τ. The cancellation apparent in this channel is the same type of cancellation that will occur in TDI variables such as X, hence we refer to it as a "single-arm TDI" experiment despite the fact that it is not a LISA TDI variable.

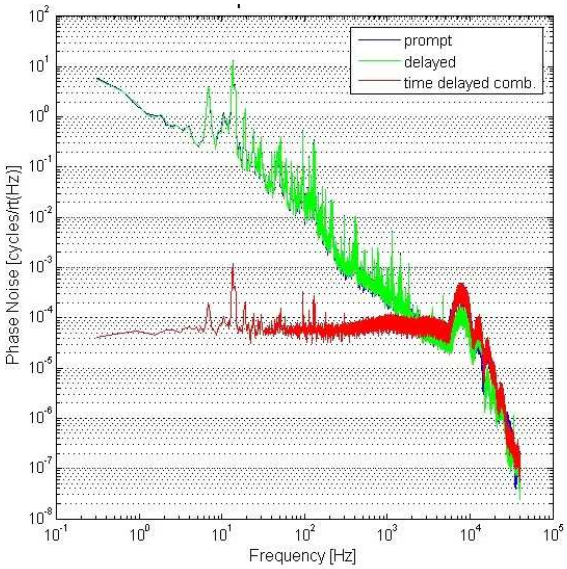

Figure 12. Results of the "single-arm TDI" experiment

The noise suppression in the TDI-like channel is not perfect, although the noise is suppressed by approximately 5 orders of magnitude at low frequencies. Possible sources for the additional noise include discrepancies between τ and τ', noise in the phasemeters, and noise added by the EPD unit. With the exception of the latter, these noise sources will also be present in LISA. The accuracy of $\tau\prime$, which will result from an independent ranging measurement between the SC, is particularly important in setting the limits on TDI.

Coupled with the requirement of accurately estimating τ is the ability to precisely generate signals such as $S(t - \tau\prime)$ from signals that are sampled at regular intervals. Without some form of interpolation, a timing error, $\Delta\tau \equiv \tau - \tau\prime$, will result that will range from zero to one-half a sample period. The noise floor present in Figure 12 is consistent with $\Delta\tau \equiv \tau - \tau\prime \approx 2\,\mu$s, consistent with the sampling period of 12.5 μs

for the phasemeters used in this experiment. Improvements can be made using fractional-delay filtering to interpolate between points, such as was used in the phasemeter results of Figure 10.

B. Arm-Locking

1) Electronic Model: An initial proof-of-concept demonstration modeling arm-locking using the EPD technique was made with a purely electronic model of a LISA arm [16], as shown in Figure 13. A voltage-controlled oscillator (VCO) stands in for the laser. The output of the VCO is split into two parts, one of which is delayed by 500 ms in an EPD unit, representing the round-trip travel along a LISA arm. These two signals are then electronically mixed, simulating the optical mixing that occurs on the LISA PD. The output of the mixer is filtered and shaped in a controller before being fed back to the actuator on the VCO.

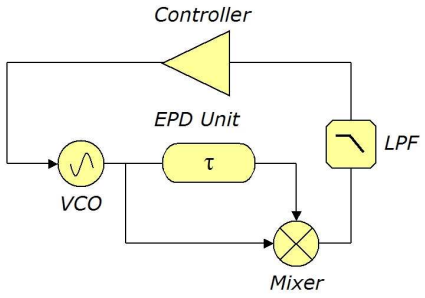

Figure 13. A purely electronic model of arm-locking in LISA

The performance of the electronic arm-locking model is shown in Figure 14. The solid red curve shows the measured ratio of stabilized to free-running noise. The dashed blue curve shows a model of the noise suppression that was fit to the data with two free parameters: the delay time in the EPD and the overall gain of the loop. The data fits the model well, showing the general character of the expected LISA arm-locking loop from Figure 6.

2) Initial Optical Model: The next step in modeling arm-locking for LISA is to include laser systems [17]. Figure 15 shows the experimental layout for the initial optical arm-locking model. The first step is to create a laser with the same noise characteristics as a pre-stabilized laser but with the ability to be tuned in frequency. To achieve this, L_1 is stabilized to an optical cavity in the standard fashion and L_2 is phase-locked to L_1 with a phase offset provided by a VCO. For a high-gain phase-lock loop, the phase of L_2 tracks the sum of the L_1 phase and the VCO phase. The free-running VCO phase noise is much smaller than the stabilized phase noise of L_1 and consequently does not increase the phase noise of L_2. L_2 is then interfered with a second pre-stabilized laser, L_0, producing a signal that is the equivalent of the LISA laser or the VCO in Figure 13. The error signal is formed using

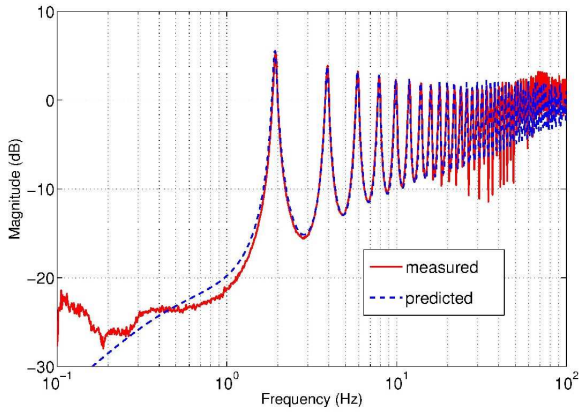

Figure 14. Closed-loop noise suppression for an electronic model of arm-locking

an EPD unit with a 1 ms delay and an electronic mixer. This small delay was necessary due to dynamic range limitations of the phasemeter used in the system. The error signal is shaped by the controller and fed into the VCO, completing the loop.

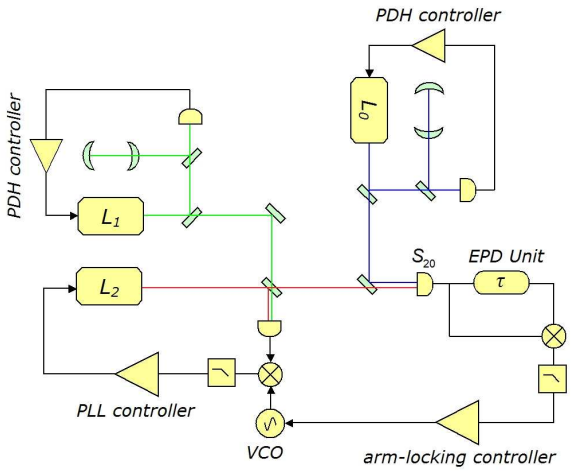

Figure 15. Experimental layout for the initial optical model of arm-locking

Figure 16 shows the performance of the initial optical arm-locking model. The measured noise suppression is shown in blue, while the result predicted from an analytic model is shown in red. While the data is not as clean as for the electronic model, it clearly follows the correct general shape, with the first few noise enhancement peaks clearly visible. The divergence from the model at high frequencies is an artifact due to the limited performance of the phasemeter used to make these measurements. At low-frequencies, the suppression appears to hit a noise floor of approximately -40 dB.

VI. Future Work

The results shown in the previous two sections demonstrate the possibilities of the EPD approach to modeling LISA. As

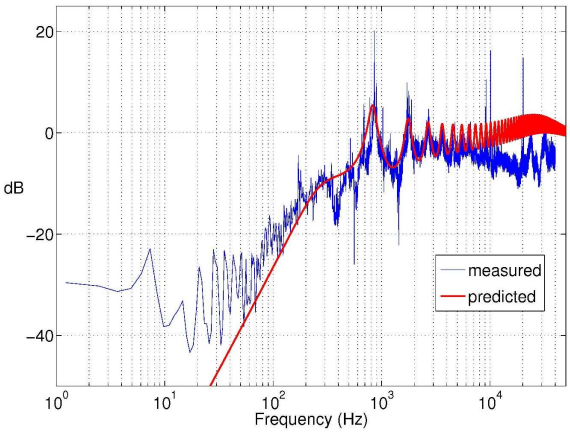

Figure 16. Results of the initial optical arm-locking model

additional improvements are made to simulator technology such as EPD units and phasemeters, the UFLIS model will improve its correlation with LISA. Our current work is focusing on generating the two-arm TDI variable X and improving the optical arm-locking model with increased noise suppression, better dynamic range, and longer delay times. Progress towards both of these goals has already been made.

Beyond these immediate goals, the UFLIS team will continue to add to the accuracy and complexity of the hardware model. This may include integrated arm-locking/TDI measurements, the addition of GW signals, and modeling of the orbital dynamics of the constellation. We believe that hardware modeling of LISA is an important activity that is complimentary to the extensive software modeling that is ongoing in the LISA data analysis community. The software models can improve UFLIS by providing details of the orbits, signals, and other effects while UFLIS will provide laboratory measurements of instrumental noise that will improve the noise modeling of the software simulators. Together with rigorous and careful testing of the LISA flight hardware, these techniques can provide the LISA team with the confidence they need to launch what promises to be a truly ground-breaking mission.

ACKNOWLEDGMENTS

This work is supported by NASA/OSS grant BEFS04-0019-0019. R.J. Cruz would like to acknowledge the Harriet Jenkins Pre-doctoral Fellowship program. J.I. Thorpe acknowledges the support of the University of Florida Alumni Fellowship.

REFERENCES

[1] B. Schutz, "Gravitational wave astronomy," *Class. Quantum Grav.*, vol. 16, pp. A131–A156, 1999.

[2] A. Abromovici and et. al., "The laser interferometer gravitational-wave observatory," *Science*, vol. 256, pp. 325–333, April 1992.

[3] P. Bender, K. Danzmann, and the LISA Study Team, "Laser interferometer space antenna for the detection of graviational waves, pre-phase a report," Max-Planck-Institut fur Quantenoptik, Garching, Tech. Rep. MPQ233, 1998, 2nd ed.

[4] L. Carbone and et al., "Characterization of disturbance sources for lisa: torsion pendulum results," *Class. Quantum Grav.*, vol. 22, pp. S509–S519, 2005.

[5] M. Tinto, D. Shaddock, J. Sylvestre, and J. Armstrong, "Implementation of time-delay interferometry for lisa," *Physical Review D*, vol. 67, no. 122003, pp. 1–17, 2003.

[6] E. Black, "An introduction to pound-drever-hall laser frequency stabilization," *Am. Jour. Phys.*, vol. 69, no. 1, pp. 79–87, January 2001.

[7] G. Mueller, P. McNamara, J. Thorpe, and J. Camp, "Laser frequency stabilization for lisa," NASA, Tech. Rep. NASA/TM-2005-212794, December 2005.

[8] B. Sheard, M. Gray, D. McClelland, and D. Shaddock, "Laser frequency stabilization by locking to a lisa arm," *Phys. Lett. A*, vol. 320, no. 1, pp. 9–21, 2003.

[9] R. Cruz and et al, "The lisa benchtop simulator at the university of florida," *Class. Quantum Grav.*, vol. 23, pp. S761–S767, 2006.

[10] R. J. Cruz, "Development of the uf lisa benchtop simulator for time delay interferometry," Ph.D. dissertation, The University of Florida, May 2006.

[11] J. I. Thorpe, "Laboratory studies of arm-locking using the laser interferometry space antenna simulator at the university of florida," Ph.D. dissertation, The University of Florida, December 2006.

[12] J. Thorpe, R. Cruz, S. Sankar, and G. Mueller, "Electronic phase delay - a first step towards a bench-top model of lisa," *Class. Quantum Grav.*, vol. 22, pp. S227–S234, 2005.

[13] D. Shaddock, B. Ware, P. Halverson, R. Spero, and B. Klipstein, "An overview of the lisa phasemeter," in *Proceedings of the Sixth International LISA Symposium*, Merkowitz and Livas, Eds., no. 873. AIP Conference Proceedings, 2006.

[14] T. Laakso, V. Valimaki, M. Karjalainen, and U. Laine, "Splitting the unit delay - tools for fractional delay filter design," *IEEE Signal Processing Magazine*, vol. 96, pp. 30–60, January 1996.

[15] R. Cruz, J. Thorpe, M. Hartmann, and G. Mueller, "Time delay interferometry using the uf lisa benchtop simulator," in *Proceedings of the Sixth International LISA Symposium*, Merkowitz and Livas, Eds., no. 873. AIP Conference Proceedings, 2006.

[16] J. Thorpe and G. Mueller, "Experimental verification of arm-locking for lisa using electronic phase delay," *Physics Lett. A*, vol. 342, pp. 199–204, 2005.

[17] J. Thorpe, R. Cruz, M. Hartmann, and G. Mueller, "Arm-locking in a lisa-like hardware model: A status report," in *Proceedings of the Sixth International LISA Symposium*, Merkowitz and Livas, Eds., no. 873. AIP Conference Proceedings, 2006.